ORIGINAL ARTICLE

A Novel Radiogenomics Biomarker for Predicting Treatment Response and Pneumotoxicity From Programmed Cell Death Protein or Ligand-1 Inhibition Immunotherapy in NSCLC

Mitchell Chen, DPhil,[a,b] Haonan Lu, PhD,[a] Susan J. Copley, MD,[a,b] Yidong Han, MMed,[b] Andrew Logan, PhD,[b] Patrizia Viola, MD,[c] Alessio Cortellini, PhD,[a,b] David J. Pinato, PhD,[a,b,d] Danielle Power, FRCR,[b] Eric O. Aboagye, PhD[a,*]

[a]*Department of Surgery and Cancer, Imperial College, London, United Kingdom*
[b]*Imperial College Healthcare NHS Trust, Hammersmith Hospital, London, United Kingdom*
[c]*North West London Pathology, Charing Cross Hospital, London, United Kingdom*
[d]*Division of Oncology, Department of Translational Medicine, University of Piemonte Orientale, Novara, Italy*

Received 25 June 2022; revised 23 November 2022; accepted 17 January 2023
Available online - XXX

ABSTRACT

Introduction: Patient selection for checkpoint inhibitor immunotherapy is currently guided by programmed death-ligand 1 (PD-L1) expression obtained from immunohistochemical staining of tumor tissue samples. This approach is susceptible to limitations resulting from the dynamic and heterogeneous nature of cancer cells and the invasiveness of the tissue sampling procedure. To address these challenges, we developed a novel computed tomography (CT) radiomic-based signature for predicting disease response in patients with NSCLC undergoing programmed cell death protein 1 (PD-1) or PD-L1 checkpoint inhibitor immunotherapy.

Methods: This retrospective study comprises a total of 194 patients with suitable CT scans out of 340. Using the radiomic features computed from segmented tumors on a *discovery* set of 85 contrast-enhanced chest CTs of patients diagnosed with having NSCLC and their *CD274* count, RNA expression of the protein-encoding gene for PD-L1, as the response vector, we developed a composite radiomic signature, lung cancer immunotherapy—radiomics prediction vector (LCI-RPV). This was validated in two independent *testing* cohorts of 66 and 43 patients with NSCLC treated with PD-1 or PD-L1 inhibition immunotherapy, respectively.

Results: LCI-RPV predicted PD-L1 positivity in both NSCLC *testing* cohorts (area under the curve [AUC] = 0.70, 95% confidence interval [CI]: 0.57–0.84 and AUC = 0.70, 95% CI: 0.46–0.94). In one cohort, it also demonstrated good prediction of cases with high PD-L1 expression exceeding key treatment thresholds (>50%: AUC = 0.72, 95% CI: 0.59–0.85 and >90%: AUC = 0.66, 95% CI: 0.45–0.88), the tumor's objective response to treatment at 3 months (AUC = 0.68, 95% CI: 0.52–0.85), and pneumonitis occurrence (AUC = 0.64, 95% CI: 0.48–0.80). LCI-RPV achieved statistically significant stratification of the patients into a high- and low-risk survival group (hazard ratio = 2.26, 95% CI: 1.21–4.24, $p = 0.011$ and hazard ratio = 2.45, 95% CI: 1.07–5.65, $p = 0.035$).

Conclusions: A CT radiomics-based signature developed from response vector *CD274* can aid in evaluating patients' suitability for PD-1 or PD-L1 checkpoint inhibitor immunotherapy in NSCLC.

*Corresponding author.

Disclosure: Dr. Pinato received lecture fees from ViiV Healthcare, Bayer Healthcare, Bristol-Myers Squibb, Roche, EISAI, and Falk Foundation; travel expenses from Bristol-Myers Squibb and Bayer Healthcare; consulting fees for Mina Therapeutics, EISAI, Roche, Avamune, Exact Sciences, Mursla, DaVolterra, and AstraZeneca; and research funding (to institution) from Merck Sharp & Dohme and Bristol-Myers Squibb. Dr. Aboagye is an advisor to Radiopharm Theranostic Ltd. The remaining authors declare no conflict of interest.

Address for correspondence: Eric O. Aboagye, PhD, Cancer Imaging Cancer, Department of Surgery and Cancer, Imperial College, Room GN1 Commonwealth Building, Du Cane Road, Hammersmith Campus, London W12 0NN, United Kingdom. E-mail: eric.aboagye@imperial.ac.uk

ISSN: 1556-0864

https://doi.org/10.1016/j.jtho.2023.01.089

Keywords: Non–small cell lung cancer; Immunotherapy; Radiomics; Pneumonitis; Prognostication

Introduction

Recent advances in checkpoint inhibition immunotherapy have redefined the landscape for treating unresectable, advanced NSCLC.[1,2] The topic of identifying cases amenable to treatment is an important one, for selecting the best treatment option and avoiding exposing patients to unnecessary treatment complications and costs. Currently, the mainstay of immunotherapy for NSCLC is the inhibition of the programmed cell death protein 1 (PD-1) or programmed death-ligand 1 (PD-L1).[3] The current practice for selecting patients for PD-1 or PD-L1 blockade is by performing histologic sampling of the tumor through percutaneous lung biopsy, endobronchial ultrasound-guided biopsy, or surgical resection, followed by immunostaining the sample to measure the percentage of cancer cells expressing PD-L1.[4] Tumor-infiltrating immune cell sampling from biopsies, however, suffers from significant sampling heterogeneity, so immunohistochemistry of the sampled tissue is not always predictive of the immune expression in the whole tumor.[5] In addition, repeated biopsies might be required as immune status can evolve over time due to tumor mutations.[5] Finally, tissue sampling can be hindered by patient's level of tolerance to the procedure, and the quantity and quality of tissue samples obtained.[6] Clinically, a PD-L1 positivity threshold of 1% is applied to determine the use of PD-1 inhibitors such as pembrolizumab and nivolumab.[7,8] Because PD-L1 expression is a dynamic and variable quantity, adopting such a positivity threshold is thought to be overly simplistic.[9] Treatment decisions guided by PD-L1 expression can also be affected by measurement variability resulting from the specific immunohistochemistry assay used.[9] Therefore, a better way of selecting NSCLC patients for PD-1 or PD-L1 inhibition immunotherapy is warranted.

Radiomic features are first- or higher-order metrics that capture quantitative information present in the imaging data. They form an active field of study in computational medical imaging, given their noninvasive nature and ability to convey important disease information not otherwise visible to human observers.[10,11] Previous studies have investigated the use of radiomics in NSCLC, including for the assessment of immune inflammatory status of the tumor, believed to play a pivotal role in differentiating the likely responders to immunotherapy from the nonresponders.[12–16] In this study, we develop a novel radiomics-based predictive model for patients with NSCLC undergoing PD-1 or PD-L1 blockade immunotherapy, using *CD274*, the protein-encoding gene for PD-L1, as the response vector.

Materials and Methods

Study Data

This is a retrospective observational study adhering to the STROBE guidelines.

The *discovery* cohort consists of 85 adult patients (age: 70.0 ± 19.1 y, male:female [M:F] = 54:31) with a histologically confirmed diagnosis of NSCLC and publicly available radiological and genomics data, including contrast-enhanced computed tomography (CT) and RNA sequencing data. It includes all eligible patients from five public domain data sets from the United States on The Cancer Imaging Archive, namely, NSCLC Radiogenomics, Clinical Proteomic Tumor Analysis Consortium squamous cell carcinoma, adenocarcinoma, and the Cancer Genome Atlas Program squamous cell carcinoma, and adenocarcinoma data sets.[12,17,18] Exclusion criteria include missing clinical data or contrast-enhanced CT scans of the tumor with a transverse spatial resolution of less than 3 mm. These data were drawn from several institutions in the United States, acquired on a range of scanners. The study aim was to develop a model on a heterogeneous cohort that is robust to variations of scanner or institutional scanning protocol and capable to withstand external testing with independent data. The *discovery* cohort was split into *training* and *internal validation* sets in a 2:1 ratio, balanced for patient's age, sex, and survival characteristics.

Two *external testing* cohorts of patients with NSCLC treated with immunotherapy were used for study validation.

The first cohort, ICHNT, consists of patients recruited in a retrospective, observational study at our multicenter institution, approved by the Regional Research Ethics Committee (18HH4616). A total of 66 (age: 67.4 ± 9.4 y, M:F = 43:23) adult patients with a diagnosis of NSCLC treated with PD-1 or PD-L1 inhibitor immunotherapy between August 2018 and December 2019 were enrolled. The scanners used were Siemens Definition AS+ and Philips Ingenuity.

The second cohort, LCWES, consists of a separate group of 43 adult patients with NSCLC (age: 66.0 ± 9.5 y, M:F = 23:20) treated with PD-1 or PD-L1 inhibitor immunotherapy between February 2014 and August 2018 at the same institution, as part of an Imperial College Tissue Bank–approved study (institutional review board: 17/WA/0161/R18009). The samples were obtained from the primary tumor where possible or from the recurrent neoplasm where there was prior resection of the primary tumor (seven cases). The scans were performed on Siemens Definition AS+.

Table 1. Characteristics of Patients Included in the Study and *p* Values Revealing Statistical Differences Between the Study Cohorts

Characteristics	TCIA (n = 85)	ICHNT (n = 66)	p^a	LCWES (n = 43)	p^b
Age at diagnosis (y), mean (SD)	68.2 (9.2)	67.4 (9.4)	0.72	63.9 (9.5)	0.028
Age range	39.1-85.2	35.1-81.4		38.0-80.0	
Sex (male)	54 (65.9)	43 (65.1)	0.93	23 (53.4)	0.23
Ethnicity					
Asian	1 (1.2)	3 (4.5)	0.0005	N/A	—
Hispanic/Latino	3 (3.5)	4 (6.1)			
Unknown	68 (80.0)	21 (31.8)			
White	13 (15.2)	38 (57.6)			
Smoking history					
Never smoked	50 (58.8)	N/A	—	N/A	—
Ever smoked	30 (35.3)				
Unknown	5 (5.9)				
Histology					
Squamous cell	26 (29.4)	14 (21.2)	0.0004	5 (11.6)	0.089
Adenocarcinoma	55 (64.7)	31 (47.0)		29 (67.5)	
Nonspecific NSCLC	4 (4.7)	21 (31.8)		9 (20.9)	
Performance score[c]					
0	N/A	17 (25.8)	—	16 (37.2)	0.07
1		49 (74.2)		23 (53.5)	
2		0 (0.0)		4 (9.3)	
3		0 (0.0)		0 (0.0)	
4		0 (0.0)		0 (0.0)	
T stage[d]					
In situ	2 (2.4)	0 (0.0)	0.0008	0 (0.0)	0.005
1	33 (38.8)	3 (4.9)		1 (2.3)	
2	39 (45.9)	7 (11.5)		17 (39.5)	
3	9 (10.6)	19 (31.1)		13 (30.2)	
4	2 (2.4)	32 (52.5)		12 (28.0)	
N stage					
0	62 (72.9)	15 (22.7)	0.0004	7 (16.3)	0.15
1	16 (18.8)	4 (6.1)		4 (9.3)	
2	7 (8.2)	27 (40.9)		11 (25.6)	
3	0 (0.0)	20 (30.3)		21 (48.8)	
M stage					
0	82 (96.5)	17 (25.8)	0.0005	9 (20.9)	0.61
1	3 (3.5)	49 (74.2)		34 (79.1)	
Drug					
Atezolizumab	—	14 (21.2)	—	6 (14.0)	0.20
Durvalumab		1 (1.5)		0 (0.0)	
Nivolumab		3 (4.6)		1 (2.3)	
Pembrolizumab		48 (72.7)		36 (83.7)	
Line of therapy					
First	—	12 (18.2)	—	15 (34.9)	0.10
Second		54 (81.8)		28 (65.1)	
Other treatment					
Radiotherapy	N/A	37 (46.1)	—	N/A	—
Chemotherapy		N/A		29 (67.4)	
Curative surgery		N/A		7 (16.3)	
Treatment completion	—	22 (33.3)	—	N/A	—
Gene mutation					
EGFR[e]	N/A	2 (5.7)	—	0 (0.0)	—
KRAS[f]		15 (45.4)		21 (50.0)	
ALK		0 (0.0)		1 (2.3)	
BRAF		3 (9.1)		2 (4.8)	
PIK3CA		5 (15.6)		2 (4.8)	

(continued)

Table 1. Continued

Characteristics	TCIA (n = 85)	ICHNT (n = 66)	p^a	LCWES (n = 43)	p^b
PD-L1 %					
Negative	N/A	17 (25.8)	–	4 (9.3)	0.039
>1%		49 (74.2)		39 (90.7)	
>50%		26 (41.4)			
>90%		8 (12.1)			
Response at 3 mo[g]	–	15 (22.7)	–	N/A	–
Pneumonitis occurrence after treatment initiation	–	3 (5.0)	–	N/A	–
Overall survival at 3 y	22 (26.8)	20 (31.7)	0.0008	11 (25.6)	0.69
Scan kVp					
100	5 (5.9)	37 (56.1)	0.001	28 (65.1)	0.12
20	80 (94.1)	26 (39.4)		14 (32.6)	
140	0 (0.0)	3 (4.5)		1 (2.3)	

Note: *p* values calculated using Wilcoxon signed rank for continuous variables and chi-square tests for categorical variables. Percentage figures are given in brackets, unless otherwise specified.
[a]*p* value comparing TCIA with ICHNT.
[b]*p* value comparing LCWES with ICHNT (except for ethnicity, where that between TCIA and LCWES is illustrated).
[c]On the basis of the ECOG score.
[d]Radiological staging on the basis of the IASLC staging system, eighth edition.
[e]EGFR,[7-10] percentage figures on the basis of the cases where test result is available.
[f]KRAS homolog.
[g]Disease response at 3 months defined as either complete or partial response or when iUPD is confirmed on subsequent follow-up imaging.
ECOG, Eastern Cooperative Oncology Group; IASLC, International Association for the Study of Lung Cancer; iUPD, unconfirmed progressive disease; kVp, peak kilovoltage; N/A, data not available; PD-L1, programmed death-ligand 1.

All included scans were contrast enhanced and acquired in the portal venous phase.

The patient characteristics of the included data are presented in Table 1. The CONSORT flow diagram for patient selection is present in Supplementary Figure 1.

Immunohistochemistry

PD-L1 expression in the ICHNT cohort was assessed in-house using Ventana PD-L1 (SP263) rabbit monoclonal primary antibody (F. Hoffmann-La Roche AG, Basel, Switzerland) immunohistochemistry and verified by a board-certified pathologist (PV).[19] PD-L1 expression was assessed using tumor proportion score (TPS). A sample was considered negative when TPS is less than 1%, positive if TPS is greater than or equal to 1%, strongly positive if TPS is greater than or equal to 50% but less than 90%, and very strongly positive if TPS is greater than or equal to 90%. The ICHNT cohort was tested for PD-L1 positivity (≥1%) and high expression (≥50% and ≥90%) predictions.

In addition to Ventana, the PD-L1 expression in 25 cases (58.1%) in the LCWES cohort was obtained using the Dako PD-L1 (22C3) PharmDx assay (Agilent Technologies Inc., Santa Clara, CA). The LCWES cohort was tested for PD-L1 positivity (≥1%) prediction.

Clinical Data

Patient overall survival at 3 years was used as a study end point, in line with prior study.[20] Tumor response prediction was based on the observed partial or complete response based on the immune-based therapeutics Response Evaluation Criteria in Solid Tumors (iRECIST) criteria.[21]

Image Segmentation

Two trained clinical radiologists (MC and YH), blinded to clinical and histologic data, with 7 and 13 years of chest imaging experience, respectively, double-reviewed and segmented all scans on both mediastinal (width, 350 Hounsfield Unit [HU]; level, 40 HU) and lung windows (width, 1500 HU; level, −600 HU). The interobserver agreement of the tumor segmentations was 91%, as measured by the Dice similarity coefficient. As found in Figure 1, this included a volumetric segmentation of the tumor itself, 2-mm peritumoral annulus, and a spherical volume of interest of 10 mm in diameter judged to be representative of the background lung parenchyma in the lung lobe where the lesion is located (or from an adjacent lobe where there is no aerated part of the lobe present), using 3DSlicer 4.13.0 (3D Slicer Image Computing Platform, https://www.slicer.org/).

Data Preprocessing, Feature Extraction, and Processing

After tumor segmentation, the imaging data were preprocessed to ensure uniform voxel size of 1 × 1 × 2 mm and then comprehensively analyzed for a total of 1998 radiomic features from each scan (666 features per

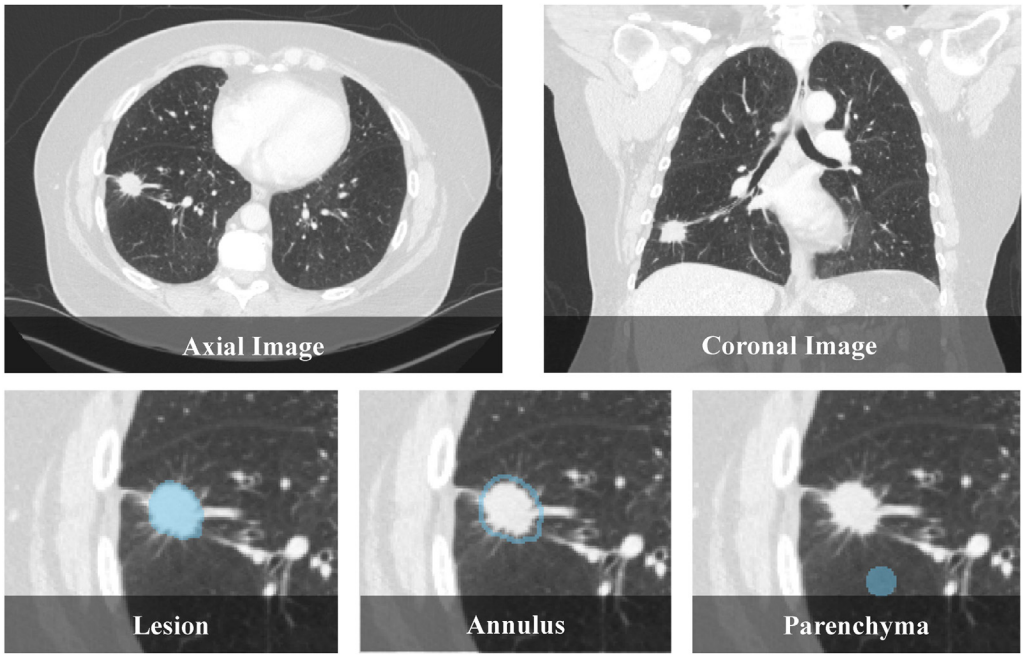

Figure 1. Segmentation method. For each case, three segmentation masks were obtained: the tumor, a 2-mm peritumoral annulus, and a spherical volume of interest of 10 mm in diameter judged to be representative of the background lung parenchyma in the lung lobe where the lesion is located or from an adjacent lobe where there is no aerated part of the lobe present.

segmentation mask), using an in-house software (TexLab 2.0), in Matlab 2020b (MathWorks Inc., Natick, MA).[22,23] The analyzed features included ones pertaining to tumor image intensity, shape, and texture, conforming to standard algorithms defined by the Image Biomarker Standardisation Initiative, where applicable.[24] The computed radiomic features were standardized to a mean of zero and SD of one. Interobserver radiomic feature reproducibility was assessed by calculating the intraclass correlation coefficient, on the basis of a two-way random model. There were 1647 features found to have an intraclass correlation coefficient greater than or equal to 0.8, thus deemed reproducible and included in the subsequent model development.

Model Development

The model was trained on the training set (n = 62) of the discovery cohort. Taking the standardized *CD274* count as the response vector, a linear regression step was applied with a false detection rate threshold of 5% to retain the most significant features (Fig. 2*A*), followed by elastic net regularization of these features plus peak kilovoltage (kVp). A composite radiogenomics signature, lung cancer immunotherapy—radiomics prediction vector (LCI-RPV), was established, as a weighted sum of 15 radiomics features deemed most relevant for *CD274* prediction (Fig. 2*B*). The signature is independent of kVp. During development, the model was validated on the internal validation set (n = 23) of the discovery cohort.

Model Validation

The model was externally tested for its prediction of PD-L1 positivity (≥1%), PD-L1 high expressions (≥50% and ≥90%), response to treatment at 3 months, and pneumonitis occurrence using receiver operating characteristic area under the curve (ROC-AUC) analysis.

The model was tested in the following two independent external testing cohorts acquired in the United Kingdom: ICHNT (n = 66), where the model was tested for its prediction of PD-L1 positivity, high PD-L1 expressions, overall survival at 3 years, tumor response at 3 months, and pneumonitis occurrence, and LCWES (n = 43), where the model was tested for its prediction of PD-L1 positivity and overall survival at 3 years.

To investigate the suitability of LCI-RPV in specific clinical situations, subcohort analyses were performed, where the biomarker was tested on the ICHNT cases stratified by the specific class of checkpoint inhibitor treatment (PD-1 or PD-L1) given the completion of the full treatment course, and whether prior radiotherapy has been administered.

The utility of the model for patient prognostication was tested, by stratifying patients into a high- and low-risk prognostic group using *k-means* clustering of LCI-RPV features.

The model development and testing framework is found in Figure 3.

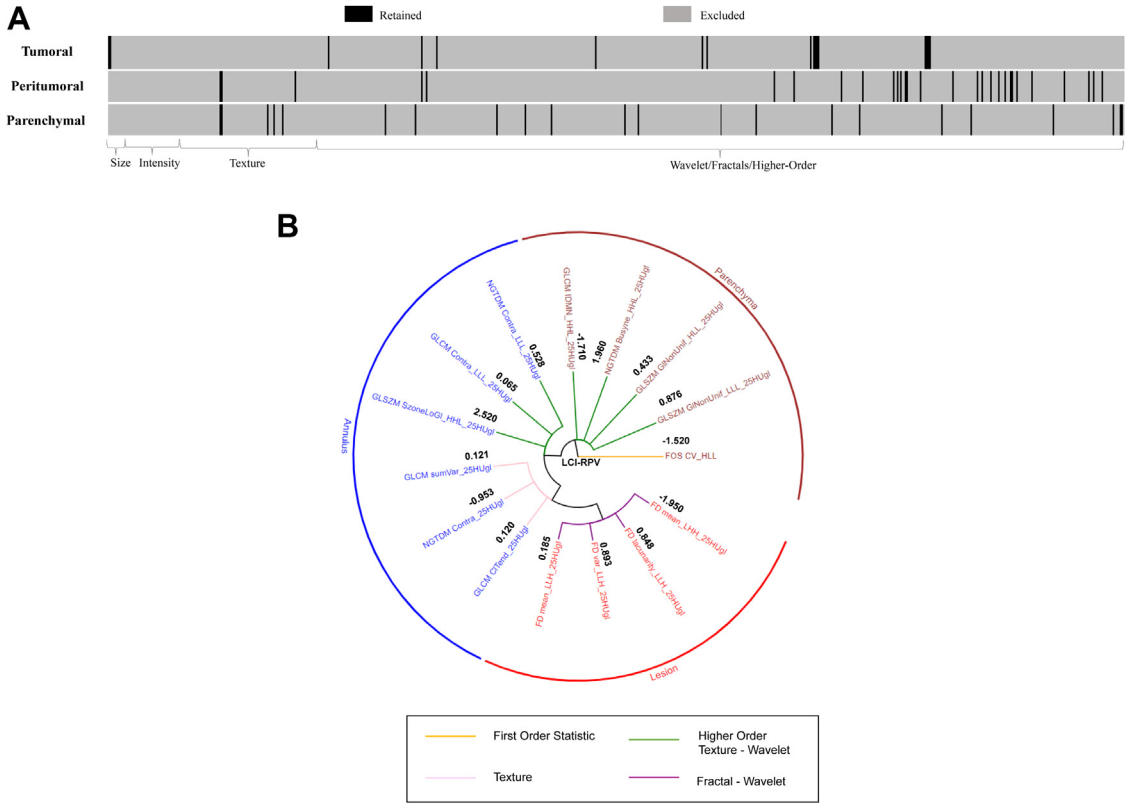

Figure 2. LCI-RPV and correlation with histologic features. (*A*) Heatmap revealing the retained features from each segmentation mask after FDR. (*B*) Phylogenetic tree revealing feature components of LCI-RPV. The feature origin (lesion, annulus, or parenchyma) and class (first order, texture, wavelet-texture or fractals) indexed by their corresponding colors as illustrated. FDR, false detection rate; LCI-RPV, lung cancer immunotherapy—radiomics prediction vector.

Mesoscopic Significance

A key strength of radiomics is its ability to capture mesoscopic features of the tumor which are present in the imaging data but not readily observable to the human eye. This bridges imaging ("macroscopic") with histology ("microscopic") and unfolds a new dimension for evaluating cancer structure and biology.[22]

To evaluate whether LCI-RPV is directly correlated with any observed histologic or imaging features, we have compared the LCI-RPV of cases in the *external testing cohort* ICNHT (n = 31, where histology slides were available), grouped by the presence or absence of histologic findings observed on low-magnified view (at 4x magnification) hematoxylin and eosin slides, and stratified by patients' response to treatment. The included histologic findings were histology subtype (squamous cell carcinoma or adenocarcinoma), keratinization if squamous cell carcinoma, primary growth pattern if adenocarcinoma, lymphovascular invasion, tumor necrosis, and inflammatory infiltration. All histologic findings were validated by a board-certified clinical histopathologist (PV).

Similarly, LCI-RPV was correlated with the presence of CT features associated with these histologic findings in ICHNT, namely peripheral ground glass, margin spiculation, central necrosis, and vascular invasion or lymphangitis carcinomatosis, stratified by patient's response to treatment. All CT features were independently validated by two board-certified clinical radiologists (MC and YH).

These histologic and radiological features are graphically illustrated in Supplementary Figure 3.

Gene Set Enrichment Analysis

Despite emerging evidence supporting the clinical use of PD-1 or PD-L1 inhibition immunotherapy for NSCLC, we are yet to fully understand its mechanism of action, particularly on how it interacts with the tumoral microenvironment to trigger an immune response against the malignancy. For example, several downstream signaling pathways are existent after ligand receptor binding and PD-L1 is expressed on more than one immune cell population with varied expression within each of such cell types.[25] An advancement of knowledge in this domain can be useful for explaining the varied response and resistance to the treatment despite positive PD-L1 expression. To investigate this, we performed

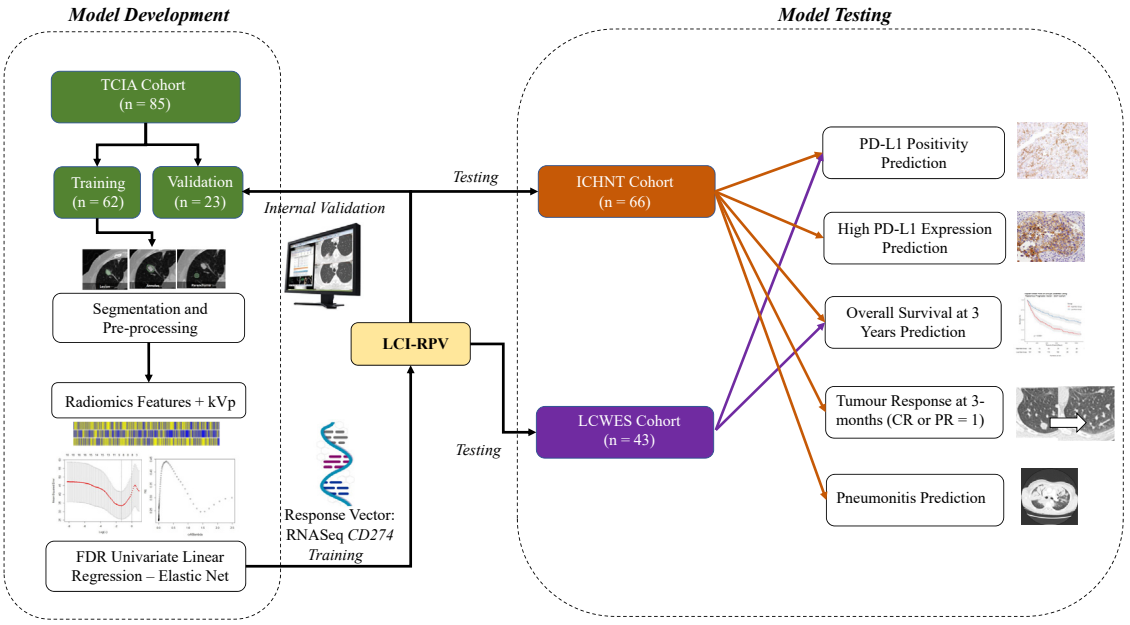

Figure 3. Study design schematics showing the key steps in model development, using *CD274* as the response vector and its validation in two independent testing cohorts. CR, complete response; FDR, false detection rate; kVp, peak kilovoltage; PD-L1, programmed death-ligand 1; PR, partial response; RNASeq, RNA sequencing.

gene set enrichment and single-cell RNA sequencing (scRNAseq) analyses to identify the enriched cellular pathways and cell populations expressing the genes most strongly correlated with our model features.

In gene set enrichment analysis (GSEA), the model feature output was correlated with the whole transcriptome from the *GSE103584* data set using Spearman's correlation.[12] The genes were ranked by their correlation coefficients and used in a preranked GSEA 4.1.0 (The Broad Institute, San Diego, CA). The Hallmark database was used for identifying enriched cellular pathways correlated with LCI-RPV.

scRNAseq Analysis

After GSEA, scRNAseq analysis was performed to identify the cell populations that express the genes which are strongly correlated with LCI-RPV. This would pave way for a better understanding of the cellular signaling basis of PD-1 pathway inhibition and how anti-tumor immunity is developed in treatment-responding cases.

The detailed steps of scRNAseq are described in the Supplementary Materials section.

Statistical Analysis

All statistical analyses and machine learning were performed using R version 4.3.0 (R Project for Statistical Computing, http://www.r-project.org/). The statistical tests were two sided, with a p value threshold of significance at 5% adopted throughout. Differences between cohorts were tested using the analysis of variance test for continuous variables and the chi-square test for categorical variables. Survival analyses were performed using Cox proportional hazard model, Kaplan-Meier survival estimates, and the log-rank test.

Results

Patient age, tumor histologic subtype, TNM stage, patient survival, and kVp were statistically significantly different between the *discovery* and *testing* cohorts, revealing the independence of the testing data to training.

Good predictive value of LCI-RPV for PD-L1 expression positivity was reported in both NSCLC *testing* cohorts (area under the curve [AUC] = 0.70, 95% confidence interval [CI]: 0.57–0.84 and AUC = 0.70, 95% CI: 0.46–0.94, for ICHNT and LCWES, found in Fig. 4*A* and *B*, respectively). In the ICHNT cohort, LCI-RPV also had good prediction of cases with high PD-L1 expression (>50%: AUC = 0.72, 95% CI: 0.59–0.85 and >90%: AUC = 0.66, 95% CI: 0.45–0.88).

The model revealed reasonable predictions of the tumor's objective response to treatment at 3 months (AUC = 0.68, 95% CI: 0.52–0.85) and pneumonitis occurrence (AUC = 0.64, 95% CI: 0.48–0.80) in ICHNT (Fig. 4*C* and *D*). Nevertheless, we note that the lower 95% CI crosses the chance threshold (0.50) in the latter case. For comparison, the predictions of tumor response at 3 months and pneumonitis occurrence using PD-L1 expression were AUC = 0.64, 95% CI: 0.47–0.81 and AUC = 0.53, 95% CI: 0.27–0.79, respectively.

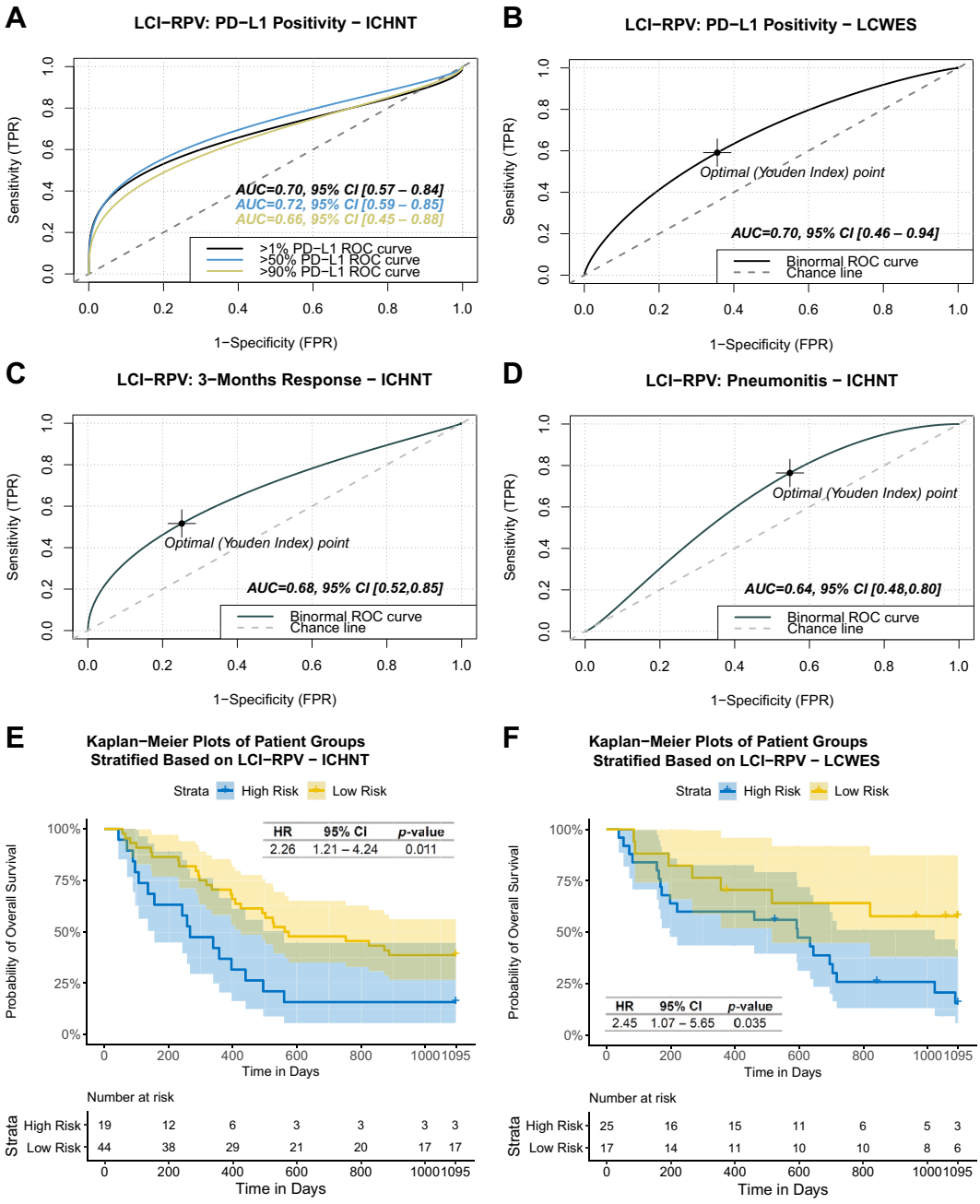

Figure 4. Predictive performance of LCI-RPV. LCI-RPV prediction of PD-L1 positivity in (*A*) the ICHNT cohort, which also includes the prediction of high PD-L1 expression (≥50% and ≥90%) cases, and (*B*) the LCWES cohort. In the ICHNT cohort, (*C*) LCI-RPV prediction of treatment response at 3 months and (*D*) pneumonitis occurrence after treatment initiation. The stratification of patients in (*E*) the ICHNT cohort and (*F*) the LCWES cohort into a high- and low-risk group based their overall survival within 3 years from the time of treatment, on the basis of their LCI-RPV signature; there were three and two entries with missing survival data in the ICHNT and LCWES cohorts, respectively, which were therefore not included in these plots. AUC, area under the curve; CI, confidence interval; FPR, false positive rate; HR, hazard ratio; LCI-RPV, lung cancer immunotherapy—radiomics prediction vector; PD-L1, programmed death-ligand 1; TPR, true positive rate.

Subcohort analysis (Supplementary Table S1) revealed superior predictive performances of LCI-RPV for tumor's response to treatment at 3 months in cases without prior treatment with radiotherapy (AUC = 0.74, 95% CI: 0.54–0.94) and of immunotherapy-associated pneumonitis in tumors treated with PD-L1 inhibitors (AUC = 0.74, 95% CI: 0.53–0.95). For comparison, worse predictive performance was observed in the group with prior radiotherapy of their cancer, where AUC = 0.55, 95% CI: 0.27–0.74 was observed for 3-month response prediction.

Statistically significant stratification of the patients into a high- and low-risk group was reported on the

basis of LCI-RPV in both *testing* cohorts (hazard ratio = 2.26, 95% CI: 1.21–4.24, $p = 0.011$ and hazard ratio = 2.45, 95% CI: 1.07–5.65, $p = 0.035$), as found in Figure 4*E* and *F*.

No responders had lymphovascular invasion on histology, or vascular invasion or lymphangitis on CT, precluding a conclusive correlation analysis in these groups. No statistically significant difference was found between the cases presenting with or without the observed histologic or radiological features, stratified by their response to immunotherapy (full results are presented in Supplementary Figs. 4 and 5).

GSEA revealed that cellular pathways emphasized in LCI-RPV–high tumors are mostly those pertaining to tissue hypoxia or inflammation (Fig. 5*A* and *B*, Supplementary Fig. 2 and Supplementary Table S2). Furthermore, pathways associated with cellular apoptosis, such as p53 and apoptosis, have been identified (Supplementary Table S3).

T and myeloid cells represented the largest clusters in t-distributed stochastic neighbor embedding (t-SNE) analysis (Fig. 5*C*). *RECOL*, *MAFB*, *SPI1*, and *FCGR3A* were among the genes with the highest correlation with LCI-RPV (Fig. 5*D*). Notably, scRNAseq analysis revealed that these four genes were highly expressed in myeloid cells, with *MAFB* and *SPI1* almost exclusively expressed in this population. *RECOL* and *FCGR3A* were also found to be frequently expressed in T cells.

Discussion

PD-1 checkpoint blockade has revolutionized systemic therapy of NSCLC. Pretreatment PD-L1 tissue expression guides treatment decision in patients with metastasis.[1] Nevertheless, response and long-term survivorship from PD-1 pathway inhibition are not exclusively linked to PD-L1 expression, highlighting the inherent limitations in the current method of patient selection for immunotherapy in NSCLC. To tackle this challenge, we developed a novel, noninvasive, radiogenomics composite biomarker for guiding clinical decisions using only CT data. It was found to have good performances for predicting PD-L1 positivity, disease response at 3 months, and pneumonitis occurrence. Notably, LCI-RPV predicted cases with high PD-L1 expression, supporting a potential role in guiding treatment decisions. The biomarker also achieved prognostic stratification in these patients. The heterogeneity of our *external testing* data (acquired on multiple scanners, at multiple sites, and in different contrast phases) strengthened our model validation.

Furthermore, LCI-RPV uniquely predicted immunotherapy-associated pneumonitis, a potentially life-threatening complication occurring in up to 5% to 20% of patients treated with checkpoint inhibitors, for which no clear mechanism nor reliable predictors exist.[26] This is a notable potential utility of LCI-RPV that is supported by findings from early pilot studies,[27,28] which is not otherwise achievable in current clinical practice. The pathogenesis of pneumonitis is poorly understood and often extrapolated from spontaneous autoimmunity or idiopathic inflammatory conditions. Whether this is due to the influence of lesional or perilesional *CD274* expression per se or the inclusion of a lung parenchymal patch in LCI-RPV remains to be elucidated. Previous work has correlated phenotypic characteristics of the T-cell infiltrate with immunotoxicity from checkpoint inhibitors.[29] In addition, immune-related adverse events are known to be enriched in immunotherapy responders, suggesting that LCI-RPV might identify a subset of patients with preexisting T-cell autoreactivity.[26] The predictive performance for pneumonitis is more pronounced in cases treated with PD-L1 inhibitors, which might be explained by the fact that the model was developed on the basis of *CD274*, the protein-encoding gene for PD-L1, and is therefore more directly related to PD-L1 than PD-1 inhibition.

Previously, radiomic features have been found to be predictive of some histologic features. For example, a composite vector of *glcm variance* and *75th percentile histogram* features was found to be predictive of micropapillary and solid growth patterns in resectable adenocarcinoma.[30] In our work, we did not find any statistically significant differences between cases presenting with and without histologic and characteristic radiological features, stratified by their response to immunotherapy. It is important to note, that because LCI-RPV was developed for *CD274* to predict for clinical outcomes in patients treated with PD-1 or PD-L1 inhibition immunotherapy, different features could have been selected in our model development than the ones predictive of histologic features. Furthermore, the small sample size (n = 31) would have limited the scope and power of this arm of the analysis.

Our pioneering work on using GSEA and scRNAseq to establish radiomic-pathology correlates offers new insight into advancing our understanding of the underlying immunobiology in PD-1 or PD-L1 pathway inhibition. Specifically, GSEA revealed that LCI-RPV is strongly associated with inflammation and hypoxia-associated gene set pathways, which was expected because a responding tumor tends to have sustained immune response through up-regulated inflammation. This finding is therefore consistent with the understanding that tissue inflammation and hypoxia play a central role in tumor response to checkpoint blockade immunotherapy.[13,31]

From scRNAseq analysis, myeloid cells were found to be a main cell type expressing genes that are highly correlated with LCI-RPV, suggesting that their

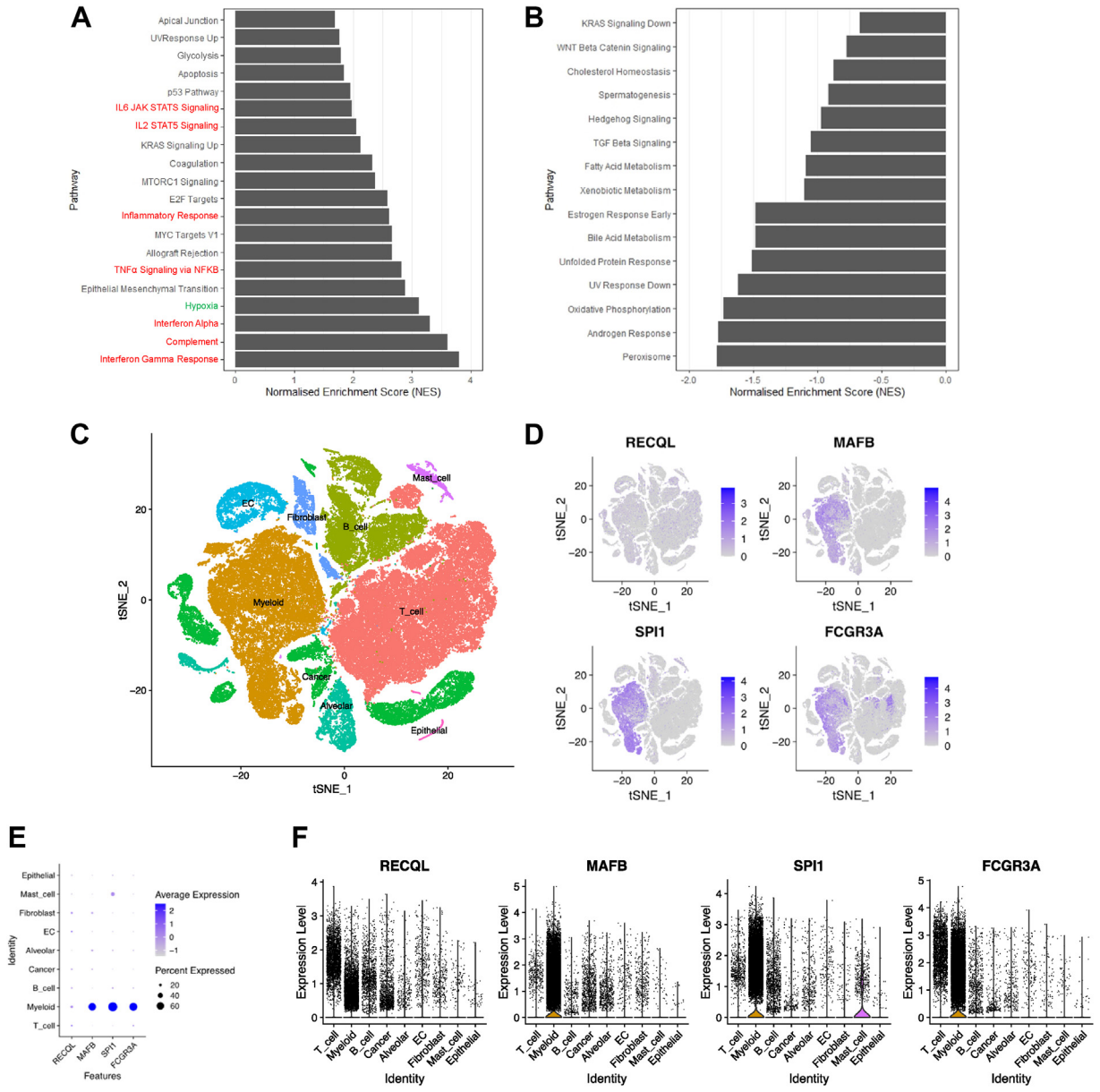

Figure 5. GSEA and scRNAseq analyses findings. Barplot revealing (*A*) the most positively correlated cellular pathways with LCI-RPV as ranked by their NES and (*B*) the most negatively correlated pathways. Note that many of the most positively correlated pathways were inflammation (red) or hypoxia related (green), a finding consistent with the immunobiological understanding that a responding tumor tends to have a sustained immune response through up-regulated inflammation. Single-cell RNA sequencing analyses findings: (*C*) t-SNE plot of 89,788 single cells from eight patients with lung cancer. (*D*) Distribution of expression of four top correlated genes (*RECQL*, *MAFB*, *SPI1*, and *FCGR3A*) with radiomic vector. (*E*) Average expression of the four genes across cell subtypes. Note the myeloid cells were most highly expressed across all four genes. (*F*) Violin plots of the four genes across cell subtypes. Note the myeloid cells were most highly expressed across all four genes. EC, enterochromaffin cell; GSEA, gene set enrichment analysis; LCI-RPV, lung cancer immunotherapy—radiomics prediction vector; NES, normalized enrichment score; scRNAseq, single-cell RNA sequencing; t-SNE, t-distributed stochastic neighbor embedding.

localization and abundance may contribute to the radiomics vector. More recently, the major contribution of PD-1 expression by myeloid cells in determining the effectiveness of immune checkpoint therapy has come to the fore.[32] Tumor-stimulated myeloid cell production, emergency myelopoiesis, is the basis of myeloid-derived suppressor cells in the tumor microenvironment; reprogramming of emergency myelopoiesis substantially affects antitumor immunity.[32] Our study provides auxiliary evidence to support this hypothesis and advances our understanding of the cellular basis of the LCI-RPV phenotype.

Evaluating the radiomic features in our developed model to appreciate the biophysical measures, we note that the features are derived from all three segmentation masks. They include fractal dimension (FD) features from the tumor itself, texture, and wavelet features from the perilesional annulus and lung parenchyma, with the most weighted one being a *glszm*-wavelet feature from the annulus. *Glszm* quantifies gray-level zones or the number of connected voxels that share the same gray-level intensity within the image; in this specific case, *szonelogl* small-zone low gray-level emphasis will be large when many small zones of low intensity are present in the image, which would be the case when there are inflammatory changes in the perilesional region. We note that the highest FD change carries a negative weight. In a similar NSCLC immunotherapy cohort study,[31] the most informative radiomic feature, *glcm inverse difference*, was positively associated with hypoxia-related carbonic anhydrase 9 using gene-expression profiling and immunohistochemistry. Separately, in another work,[33] FD was reduced in acutely inflamed tissue, indicating a loss of the overall complexity of the cells in the tissue, and asserting the characteristics of this biophysical variable in the context of inflamed tissues. Interestingly, in our work, the contribution of the negatively weighted FD to LCI-RPV was only found in the tumoral and not perilesional region, highlighting the complexity of biophysical measures in different regions of interests.

Limitations of this study include its retrospective nature that can introduce selection bias, multiple sources of the training data which can give rise to data imbalance, and the limited size of external testing data. Further external validation is warranted.

The model was developed and tested on contrast-enhanced CT data in the portal venous phase. Given the known impact of contrast enhancement on radiomic features,[34] we sought model generalizability by training and testing cases drawn from multiple clinical practice scenarios whereby satisfactory portal venous contrast enhancement was deemed to have been achieved. The rate, volume of contrast injection, and scan delay were varied, which mirrors clinical practice where the patients' individual circumstances, such as body habitus, available intravenous access, cardiac output, and renal function, would be considered when determining the optimal contrast injection regimen ad-hoc. By adopting this approach, our model is rendered more invariant to the details of contrast injection, so long as adequate enhancement in the correct phase is achieved. Radiomic features can also be influenced by the type of CT scanner used to acquire the imaging data.[35] To improve its generalizability and robustness, we have developed and tested our model on data from various centers across the United States of America and Europe using different scanner makes and models, to achieve a model that is scanner invariant.

Future works include evaluating the prediction of disease response at longer-term follow-ups, such as at 6 months and beyond, and prediction of additional events of clinical significance including other adverse events such as colitis and thyroiditis, tumor hyperprogression,[36] or sarcoid-like reaction. These might, however, require considerably larger data sets, given the relative rarity of some of these events. The incorporation of additional patient clinical data in an integrated model[31] or metabolic imaging data are additional areas with promising preliminary results supporting further investigation.[37]

On further clinical validation, this novel, noninvasive, radiogenomics biomarker could be used to guide treatment decisions, particularly in radiotherapy-naive cases where satisfactory tissue sampling can not be achieved, such as when it is not tolerated by or deemed unsafe to the patient, inadequate sample, or equivocal pathologic result. The biomarker could see additional use in pneumonitis prediction and patient prognostic stratification, both of which can help facilitating personalized cancer care.

CRediT Authorship Contribution Statement

Mitchell Chen: Data curation, Formal analysis, Funding acquisition, Investigation, Methodology, Project administration, Resources, Software, Validation, Visualization, Writing—original draft, Writing—review and editing.

Haonan Lu: Formal analysis, Investigation, Methodology, Visualization.

Susan J. Copley: Conceptualization, Data curation, Funding acquisition, Investigation, Methodology, Project administration, Resources, Supervision, Writing—review and editing.

Yidong Han: Data curation.

Andrew Logan: Data curation.

Patrizia Viola: Data curation, Investigation, Writing—review and editing.

Alessio Cortellini: Data curation, Methodology, Writing—review and editing.

David J. Pinato: Data curation, Methodology, Writing—review and editing.

Danielle Power: Resources.

Eric O. Aboagye: Conceptualization, Funding acquisition, Investigation, Methodology, Project administration, Resources, Software, Supervision, Writing—review and editing.

Data Availability

All study data including the imaging data can be provided on reasonable request to the corresponding author.

Code Availability

The R code used to develop and validate the proposed biomarker is available on GitHub (https://github.com/scat2801/pdl1io).

Acknowledgments

This work was supported with funding from the Imperial College Biomedical Research Centre award (WSCC P87324, P62585). Furthermore, MC is supported by National Institute for Health Research Clinical Lectureship CL-2021-21-005 and Academy of Medical Sciences award SGL026\1024. DJP is supported by grant funding from the Wellcome Trust Strategic Fund (WSCC_PS3416) and from the Associazione Italiana per la Ricerca sul Cancro (AIRC MFAG Grant ID 25697). The authors acknowledge additional support from the Imperial Experimental Cancer Medicine Centre (C1312/A25149), the Imperial College Tissue Bank, UK Medical Research Council (MR/N020782/1), and UK National Cancer Imaging Translational Accelerator (C2536/A28680). The study funders did not have a role in the design and conduct of the study; collection, management, analysis, and interpretation of the data; preparation, review, or approval of the manuscript; or decision to submit the manuscript for publication. The results published here are in part based on data generated by the TCGA Research Network: https://www.cancer.gov/tcga. Data used in this publication were generated by the Clinical Proteomic Tumor Analysis Consortium (NCI/NIH). Human samples used in this research project were obtained from the Imperial College Healthcare Tissue Bank (ICHTB). ICHTB is supported by the National Institute for Health Research Biomedical Research Centre based at the Imperial College Healthcare NHS Trust and Imperial College London. ICHTB is approved by Wales REC3 to release human material for research (17/WA/0161). Data were also obtained from Imperial College Healthcare NHS Trust. The authors also acknowledge the supporting work by the Imaging Research (ImRes) team at the Imperial College Healthcare NHS Trust. Dr. Chen has full access to all the data in the study and takes responsibility for the integrity of the data and the accuracy of the data analysis.

Supplementary Data

Note: To access the supplementary material accompanying this article, visit the online version of the *Journal of Thoracic Oncology* at www.jto.org and at https://doi.org/10.1016/j.jtho.2023.01.089.

References

1. Reck M, Rodríguez-Abreu D, Robinson AG, et al. Pembrolizumab versus chemotherapy for PD-L1-positive non-small-cell lung cancer. *N Engl J Med*. 2016;375:1823–1833.
2. Borghaei H, Paz-Ares L, Horn L, et al. Nivolumab versus docetaxel in advanced nonsquamous non-small-cell lung cancer. *N Engl J Med*. 2015;373:1627–1639.
3. Arbour KC, Riely GJ. Systemic therapy for locally advanced and metastatic non-small cell lung cancer: a review. *JAMA*. 2019;322:764–774.
4. Lantuejoul S, Sound-Tsao M, Cooper WA, et al. PD-L1 testing for lung cancer in 2019: perspective from the IASLC pathology committee. *J Thorac Oncol*. 2020;15:499–519.
5. McLaughlin J, Han G, Schalper KA, et al. Quantitative assessment of the heterogeneity of PD-L1 expression in non-small-cell lung cancer. *JAMA Oncol*. 2016;2:46–54.
6. Sholl L. Molecular diagnostics of lung cancer in the clinic. *Transl Lung Cancer Res*. 2017;6:560–569.
7. Mok TSK, Wu YL, Kudaba I, et al. Pembrolizumab versus chemotherapy for previously untreated, PD-L1-expressing, locally advanced or metastatic non-small-cell lung cancer (KEYNOTE-042): a randomised, open-label, controlled, phase 3 trial. *Lancet*. 2019;393:1819–1830.
8. Hellmann MD, Paz-Ares L, Bernabe Caro R, et al. Nivolumab plus ipilimumab in advanced non-small-cell lung cancer. *N Engl J Med*. 2019;381:2020–2031.
9. Tsimafeyeu I, Imyanitov E, Zavalishina L, et al. Agreement between PDL1 immunohistochemistry assays and polymerase chain reaction in non-small cell lung cancer: CLOVER comparison study. *Sci Rep*. 2020;10:3928.
10. Aerts HJWL, Velazquez ER, Leijenaar RTH, et al. Decoding tumour phenotype by noninvasive imaging using a quantitative radiomics approach. *Nat Commun*. 2014;5:4006.
11. Lambin P, Leijenaar RTH, Deist TM, et al. Radiomics: the bridge between medical imaging and personalized medicine. *Nat Rev Clin Oncol*. 2017;14:749–762.
12. Bakr S, Gevaert O, Echegaray S, et al. A radiogenomic dataset of non-small cell lung cancer. *Sci Data*. 2018;5:180202.
13. Sun R, Limkin EJ, Vakalopoulou M, et al. A radiomics approach to assess tumour-infiltrating CD8 cells and response to anti-PD-1 or anti-PD-L1 immunotherapy: an imaging biomarker, retrospective multicohort study. *Lancet Oncol*. 2018;19:1180–1191.
14. Khorrami M, Prasanna P, Gupta A, et al. Changes in CT radiomic features associated with lymphocyte distribution predict overall survival and response to immunotherapy in non-small cell lung cancer. *Cancer Immunol Res*. 2020;8:108–119.
15. Wu M, Zhang Y, Zhang J, et al. A combined-radiomics approach of CT images to predict response to anti-PD-1 immunotherapy in NSCLC: a retrospective multicenter study. *Front Oncol*. 2022;11:688679.
16. Ligero M, Garcia-Ruiz A, Viaplana C, et al. A CT-based radiomics signature is associated with response to

immune checkpoint inhibitors in advanced solid tumors. *Radiology*. 2021;299:109–119.
17. Edwards NJ, Oberti M, Thangudu RR, et al. The CPTAC data portal: a resource for cancer proteomics research. *J Proteome Res*. 2015;14:2707–2713.
18. Hammerman PS, Voet D, Lawrence MS. Comprehensive genomic characterization of squamous cell lung cancers. *Nature*. 2012;489:519–525.
19. Elshiekh M, Spinelli M, Iles S, et al. PD-L1 testing in advanced stage lung cancer using cytology samples: suitability and reporting issues. Comparison between two tertiary referral centers. *Ann Cytol Pathol*. 2021;6(1):001-6.
20. Li Q, Kim J, Balagurunathan Y, et al. CT imaging features associated with recurrence in non-small cell lung cancer patients after stereotactic body radiotherapy. *Radiat Oncol*. 2017;12:1–10.
21. Seymour L, Bogaerts J, Perrone A, et al. iRECIST: guidelines for response criteria for use in trials testing immunotherapeutics. *Lancet Oncol*. 2017;18:e143–e152.
22. Lu H, Arshad M, Thornton A, et al. A mathematical-descriptor of tumor-mesoscopic-structure from computed-tomography images annotates prognostic- and molecular-phenotypes of epithelial ovarian cancer. *Nat Commun*. 2019;10:764.
23. Lu H, Cunnea P, Nixon K, Rinne N, Aboagye EO, Fotopoulou C. Discovery of a biomarker candidate for surgical stratification in high-grade serous ovarian cancer. *Br J Cancer*. 2021;124:1286–1293.
24. Zwanenburg A, Vallières M, Abdalah MA, et al. The image biomarker standardization initiative: standardized quantitative radiomics for high-throughput image-based phenotyping. *Radiology*. 2020;295:328–338.
25. Gaikwad S, Agrawal MY, Kaushik I, Ramachandran S, Srivastava SK. Immune checkpoint proteins: signaling mechanisms and molecular interactions in cancer immunotherapy. *Semin Cancer Biol*. 2022;86:137–150.
26. Fessas P, Possamai LA, Clark J, et al. Immunotoxicity from checkpoint inhibitor therapy: clinical features and underlying mechanisms. *Immunology*. 2020;159:167.
27. Colen RR, Fujii T, Bilen MA, et al. Radiomics to predict immunotherapy-induced pneumonitis: proof of concept. *Investig New Drugs*. 2018;36:601–607.
28. Schoenfeld JD, Nishino M, Severgnini M, Manos M, Mak RH, Hodi FS. Pneumonitis resulting from radiation and immune checkpoint blockade illustrates characteristic clinical, radiologic and circulating biomarker features. *J Immunother Cancer*. 2019;7:112.
29. Oh DY, Cham J, Zhang L, et al. Immune toxicities elicted by CTLA-4 blockade in cancer patients are associated with early diversification of the T cell repertoire. *Cancer Res*. 2017;77:1322.
30. Chen LW, Yang SM, Wang HJ, et al. Prediction of micropapillary and solid pattern in lung adenocarcinoma using radiomic values extracted from near-pure histopathological subtypes. *Eur Radiol*. 2021;31:5127–5138.
31. Tunali I, Tan Y, Gray JE, et al. Hypoxia-related radiomics and immunotherapy response: a multicohort study of non-small cell lung cancer. *JNCI Cancer Spectr*. 2021;5:kab048.
32. Strauss L, Mahmoud MAA, Weaver JD, et al. Targeted deletion of PD-1 in myeloid cells induces antitumor immunity. *Sci Immunol*. 2020;5:eaay1863.
33. Stankovic M, Pantic I, de Luca SR, et al. Quantification of structural changes in acute inflammation by fractal dimension, angular second moment and correlation. *J Microsc*. 2016;261:277–284.
34. Kakino R, Nakamura M, Mitsuyoshi T, et al. Comparison of radiomic features in diagnostic CT images with and without contrast enhancement in the delayed phase for NSCLC patients. *Phys Med*. 2020;69:176–182.
35. Mackin D, Fave X, Zhang L, et al. Measuring computed tomography scanner variability of radiomics features. *Invest Radiol*. 2015;50:757–765.
36. Vaidya P, Bera K, Patil PD, et al. Novel, non-invasive imaging approach to identify patients with advanced non-small cell lung cancer at risk of hyperprogressive disease with immune checkpoint blockade. *J Immunother Cancer*. 2020;8:e001343.
37. Mu W, Jiang L, Zhang JY, et al. Non-invasive decision support for NSCLC treatment using PET/CT radiomics. *Nat Commun*. 2020;11:5228.